Title

Surface Glycan Modification of Cellular Nanosponges to Promote SARS-CoV-2 Inhibition.

Journal

Journal of the American Chemical Society, 143(42)

ISSN

0002-7863

Authors

Ai, Xiangzhao
Wang, Dan
Honko, Anna
et al.

Publication Date

2021-10-01

DOI

10.1021/jacs.1c07798

Peer reviewed

JACS
JOURNAL OF THE AMERICAN CHEMICAL SOCIETY
pubs.acs.org/JACS
Article

Surface Glycan Modification of Cellular Nanosponges to Promote SARS-CoV-2 Inhibition

Xiangzhao Ai,[§] Dan Wang,[§] Anna Honko, Yaou Duan, Igor Gavrish, Ronnie H. Fang, Anthony Griffiths, Weiwei Gao,* and Liangfang Zhang*

Cite This: https://doi.org/10.1021/jacs.1c07798

ABSTRACT: Cellular binding and entry of severe acute respiratory syndrome coronavirus 2 (SARS-CoV-2) are mediated by its spike glycoprotein (S protein), which binds with not only the human angiotensin-converting enzyme 2 (ACE2) receptor but also glycosaminoglycans such as heparin. Cell membrane-coated nanoparticles ("cellular nanosponges") mimic the host cells to attract and neutralize SARS-CoV-2 through natural cellular receptors, leading to a broad-spectrum antiviral strategy. Herein, we show that increasing surface heparin density on the cellular nanosponges can promote their inhibition against SARS-CoV-2. Specifically, cellular nanosponges are made with azido-expressing host cell membranes followed by conjugating heparin to the nanosponge surfaces. Cellular nanosponges with a higher heparin density have a larger binding capacity with viral S proteins and a significantly higher inhibition efficacy against SARS-CoV-2 infectivity. Overall, surface glycan engineering of host-mimicking cellular nanosponges is a facile method to enhance SARS-CoV-2 inhibition. This approach can be readily generalized to promote the inhibition of other glycan-dependent viruses.

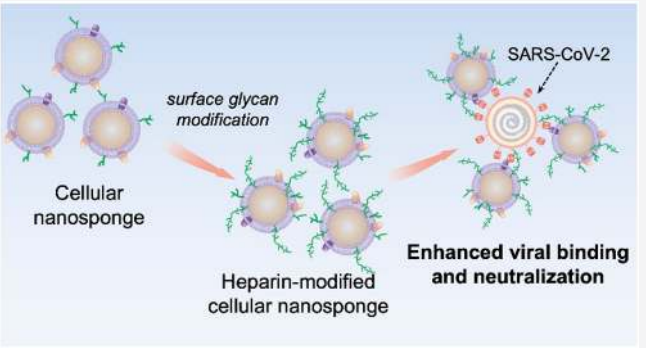

INTRODUCTION

The severe acute respiratory syndrome coronavirus 2 (SARS-CoV-2) is responsible for the current pandemic of coronavirus disease 2019 (COVID-19), a crisis with an unprecedented threat to global public health.[1−3] So far, the antiviral drugs such as remdesivir,[4] monoclonal antibodies such as bamlanivimab and etesevimab,[5] and vaccines manufactured by Pfizer-BioNTech, Moderna, and Janssen[6] have been approved as emergency-use authorization in the United States for COVID-19 treatment and prevention. However, SARS-CoV-2 can undergo genetic mutations over time, resulting in the unpredictable evolutions of new viral strains resistant to the current therapeutics or vaccines.[7−9] Therefore, innovative strategies that can inhibit the infectivity of SARS-CoV-2 and its potential mutated strains are highly demanded.

Nanomedicine platforms have shown high potential in the diagnosis, treatment, and prevention of viral infections.[10−13] Among them, cell-membrane-coated nanoparticles, namely, "cellular nanosponges", have attracted much attention. Cellular nanosponges are made by cloaking plasma membranes of the host cells onto synthetic cores. They inherit natural protein and glycan receptors from the host cells, either known or unknown, to bind with viral proteins and divert the viruses away from the intended cellular targets.[13,14] Such a working mechanism shifts the focus from the causative viruses to the hosts and thus overcomes virus diversity, limiting the traditional antiviral approach. Cellular nanosponges effectively capture and inactivate pathogenic viruses such as human immunodeficiency virus (HIV),[15] influenza virus,[16] Zika virus,[17] and recently SARS-CoV-2,[14,18,19] unlocking a broad-spectrum antiviral strategy.

During the infection, SARS-CoV-2 viruses use their spike-like proteins (S proteins) on the surface to attach to the cellular angiotensin-converting enzyme 2 (ACE2) for entering the host cells. Recent studies suggest that, before the ACE2 binding, the receptor-binding domain (RBD) of the viral S protein first interacts with the glycocalyx components of the membranes such as heparin or heparan sulfate (HS).[20] Such interactions lead to an open conformation of the S protein that enhances its subsequent binding to the ACE2.[21] This observation is further supported by SARS-CoV-2 inhibition in vitro using heparin or heparan sulfate.[22,23] Therefore, alteration of heparan sulfate on the host cell surface presents potential therapeutic opportunities against SARS-CoV-2 infection. On the basis of this scientific premise, we

Received: July 26, 2021

https://doi.org/10.1021/jacs.1c07798
J. Am. Chem. Soc. XXXX, XXX, XXX−XXX

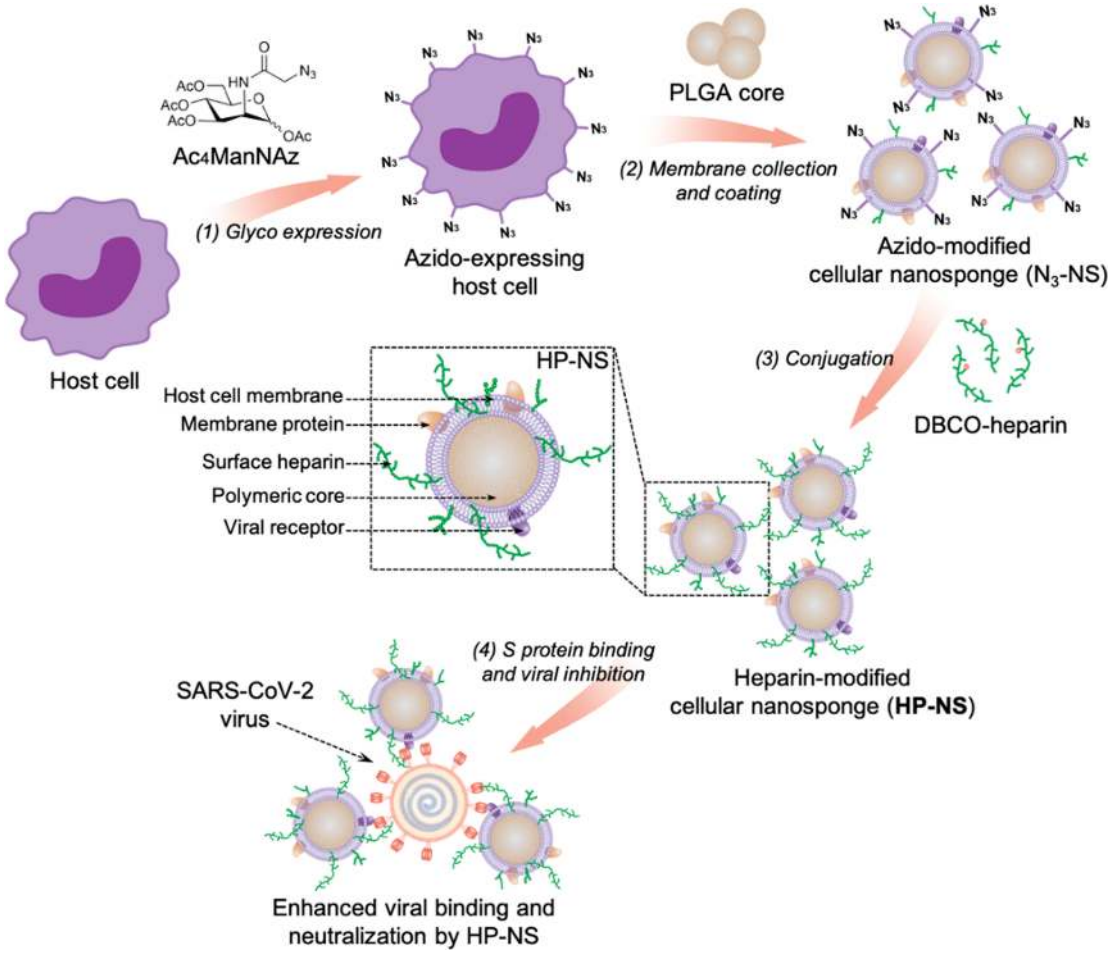

Figure 1. Schematic illustration of engineering surface glycans onto cellular nanosponges to promote SARS-CoV-2 inhibition. In the scheme, the host cells are first incubated with *N*-azidoacetylmannosamine-tetraacylated ($Ac_4ManNAz$) to express azido groups. Their membranes are collected and coated onto polymeric nanoparticle cores made of poly(lactic-*co*-glycolic acid) (PLGA) to form cellular nanosponges expressing azido groups (denoted "N_3-NS"). Then heparin functionalized with the dibenzocyclooctyne groups (DBCO-heparin) is conjugated to azido-NS through copper-free click chemistry, forming heparin-modified cellular nanosponges (denoted "HP-NS"). The HP-NS are then examined for binding ability with SARS-CoV-2 S proteins and inhibition efficacy against the viral infectivity.

hypothesize that a higher level of heparin on the cellular nanosponges will lead to a higher binding ability with the viral S protein and hence a higher inhibition efficacy against SARS-CoV-2 for host protection.

To test this hypothesis, we synthesized heparin-functionalized cellular nanosponges (denoted "HP-NS") with different heparin densities (Figure 1). To make such nanosponges, we first introduced azido groups (N_3) onto the host cell membranes through glycol expression. Next, we derived their membranes and coated them onto polymeric cores made of poly(lactic-*co*-glycolic acid) (PLGA), making cellular nanosponges expressing azido groups (denoted "N_3-NS"). We then functionalized heparin with the dibenzocyclooctyne group (DBCO-heparin) and conjugated it onto N_3-NS through copper-free click chemistry, forming HP-NS with the heparin density controlled by heparin-nanosponge stoichiometry. Lastly, we examined the capacity of HP-NS binding with SARS-CoV-2 S proteins and the efficacy of inhibiting viral infectivity. We demonstrated that HP-NS with a higher level of heparin bound more SARS-CoV-2 S proteins. Furthermore, when tested with SARS-CoV-2 pseudovirus, HP-NS with a higher level of heparin showed higher inhibition of viral infectivity. Overall, our results show that surface glycan modification is a facile strategy to boost cellular nanosponges against glycan-dependent viral threats such as SARS-CoV-2.

RESULTS AND DISCUSSION

In the study, metabolic labeling of an azido group (N_3) onto THP-1 cells, a human macrophage (MΦ) cell line, was achieved by incubating the cells with *N*-azidoacetylmannosamine-tetraacylated ($Ac_4ManNAz$). In this process, $Ac_4ManNAz$ was metabolized into *N*-azidoacetyl neuraminic acid and then incorporated into glycans for expression.[24] To confirm the expression, we measured the N_3 level on the cells before and after the incubation by tagging the N_3 group with dibenzocyclooctyne-cyanine 3 (DBCO-Cy3) via copper-free click chemistry. The cell surface N_3 level increased significantly when the cells were incubated with $Ac_4ManNAz$ (Figure 2A). However, despite a high level of N_3 expression, the cell viability showed no detectable change (Figure 2B).

After the N_3 expression, we first derived the membranes of N_3-expressing THP-1 cells and purified them using mechanical disruption and differential centrifugation.[25] Meanwhile, PLGA cores were made with a nanoprecipitation procedure by adding the polymer in an organic solvent to an aqueous phase followed by evaporation.[26] Then, cell membranes were coated

https://doi.org/10.1021/jacs.1c07798
J. Am. Chem. Soc. XXXX, XXX, XXX−XXX

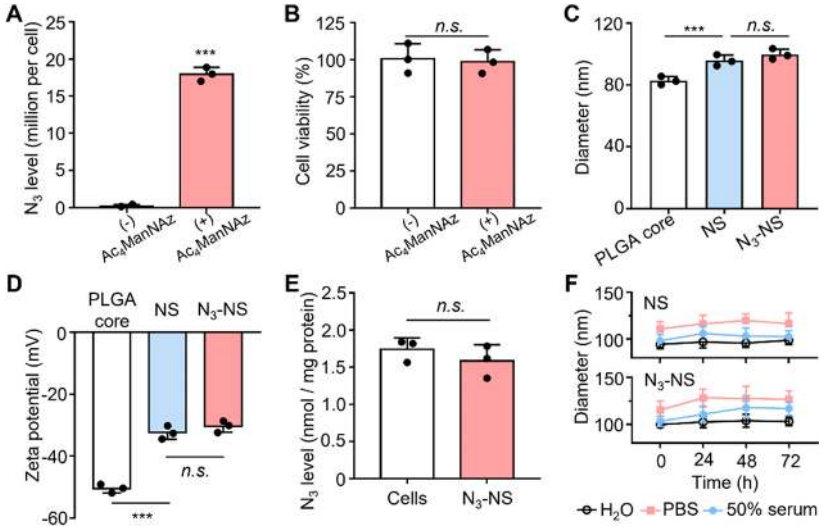

Figure 2. Formulation and characterization of azido-modified cellular nanosponges (N_3-NS). (A) Surface N_3 levels of the THP-1 cells cultured with or without Ac_4ManNAz. (B) Cell viability of THP-1 cells cultured with or without Ac_4ManNAz. (C, D) Hydrodynamic size (C, diameter) and surface zeta potential (D, mV) of the PLGA core, cellular nanosponges made with unmodified THP-1 membranes ("NS"), and N_3-NS. (E) Comparison of the N_3 levels on N_3-NS (100 μL, 1 mg/mL of membrane proteins) and source cells (100 μL, approximately 1×10^7 cells) containing equal amounts of membrane content. The N_3 levels were measured by staining the samples with DBCO-Cy3 (10 μM). (F) Hydrodynamic sizes of NS and N_3-NS in H_2O, 1× PBS, and 50% serum over 72 h. Data presented as mean + s.d. ($n = 3$); *n.s.*: not significant; ***$p < 0.001$; statistical analysis by paired *t*-test.

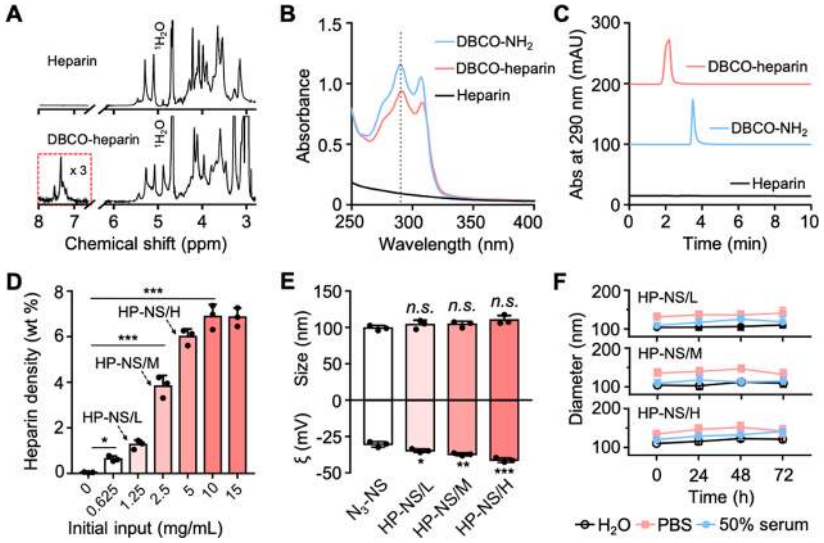

Figure 3. Fabrication and characterization of heparin-modified cellular nanosponges (HP-NS). (A) ^{1}H NMR spectrum (500 MHz) of heparin (top) and DBCO-heparin (bottom). The broad signal at 7−8 ppm corresponds to the DBCO moiety. (B, C) UV absorbance spectrum (B) and HPLC analysis (C) of heparin, DBCO-NH_2, and DBCO-heparin. (D) Relationship between DBCO-heparin initial input and heparin density on NS surfaces. Three HP-NS formulations with low, middle, and high heparin densities (denoted "HP-NS/L", "HP-NS/M", and "HP-NS/H") were chosen for the subsequent studies. (E) DLS measurements of hydrodynamic size (diameter) and zeta potential (ζ) for N_3-NS, HP-NS/L, HP-NS/M, and HP-NS/H. (F) Hydrodynamic size of HP-NS/L, HP-NS/M, and HP-NS/H in H_2O, 1× PBS, and 50% serum over 72 h. Data presented as mean + s.d. ($n = 3$); *n.s.*: not significant; ***$p < 0.001$; statistical analysis by one-way ANOVA.

onto PLGA cores with bath sonication, forming azido-expressing cellular nanosponges (denoted "N_3-NS"). Cellular nanosponges were also made with unmodified THP-1 cells (denoted "NS") as a control.

Following the formulation, dynamic light scattering (DLS) measurements revealed that NS and N_3-NS had similar hydrodynamic diameters of 95.8 ± 3.6 and 99.7 ± 3.4 nm, respectively. These values are higher than that of the uncoated PLGA cores (82.7 ± 2.2 nm), suggesting the addition of a bilayered cell membrane onto the polymeric cores (Figure 2C). Meanwhile, the surface zeta-potential of the N_3-NS (−30.4 ± 1.9 mV) was less negative than that of the PLGA cores (−50.5 ± 1.4 mV) but comparable to that of the NS (−32.4 ± 2.2 mV) (Figure 2D), likely due to the charge screening by the membrane coating. To examine the membrane sidedness, we stained the N_3-expressing THP-1 source cells and N_3-NS containing equal amounts of membrane content by using DBCO-Cy3 dye for the surface N_3 levels. After removal of the free dye, the two samples showed comparable N_3 levels (Figure 2E). This result

https://doi.org/10.1021/jacs.1c07798
J. Am. Chem. Soc. XXXX, XXX, XXX−XXX

indicated that the N_3-NS adopted a right-side-out membrane orientation because an inside-out membrane coating would have reduced the levels of N_3-labeled glycans.[15] When suspended in water, phosphate-buffered saline (PBS, 1×), and 50% serum, the sizes of NS and N_3-NS remained unchanged over 72 h, suggesting their good colloidal stability (Figure 2F). Together, these results demonstrated the successful preparation of N_3-NS.

To fabricate HP-NS, we first functionalized heparin with DBCO by conjugating DBCO-NH_2 to the carboxylic groups of the heparin, followed by purification with dialysis. In ^{1}H NMR analysis, the product spectrum showed additional peaks around approximately 7.5 ppm, consistent with DBCO (Figure 3A).[27] When analyzed with UV absorption spectroscopy, the product showed DBCO absorption at about 290−310 nm (Figure 3B).[28] Moreover, in the analysis with high-performance liquid chromatography (HPLC), the elution time of the DBCO signal (at 290 nm) from the product shifted when compared with that of DBCO-NH_2, suggesting the conjugation to the heparin polymer chain (Figure 3C). Together, these results confirm the successful synthesis of DBCO-heparin. The DBCO density (the weight percentage of DBCO in the DBCO-functionalized heparin product) was determined to be 2.3 ± 0.1 wt % based on the UV absorption spectroscopy (Supporting Information Figure S1).

Next, we formulated HP-NS by conjugating DBCO-heparin onto N_3-NS through a copper-free click chemistry reaction. When DBCO-heparin input was increased from 0 to 15 mg/mL, the heparin density on HP-NS increased but reached a plateau at an input of 10 mg/mL (Figure 3D). Based on this study, we selected three HP-NS formulations with low, middle, and high heparin densities (denoted "HP-NS/L", "HP-NS/M", and "HP-NS/H", respectively). The heparin density of the three formulations (the weight percentage of the conjugated heparin compared to the total membrane protein weight) was 0.6, 3.8, and 6.8 wt %, respectively. Heparin conjugation had little effect on the HP-NS hydrodynamic sizes (Figure 3E). However, as the heparin content increased, the zeta potential of the nanoparticles became less negative, likely due to the increased contribution of the negative charge from the heparin backbone. In addition, all three HP-NS formulations showed excellent colloidal stability in water, 1× PBS, and 50% serum, respectively (Figure 3F).

After formulating HP-NS, we then evaluated their binding capability with SARS-CoV-2 S proteins. In the study, serial dilutions of HP-NS were mixed with the S proteins (recombinant S1 subunit). After the incubation, HP-NS were removed with ultracentrifugation, and the unbound S protein concentration in the supernatant was quantified. As shown in Figure 4A, when the amounts of HP-NS increased, the concentration of the unbound S protein decreased, suggesting a dose-dependent S protein neutralization of all three HP-NS formulations. At each HP-NS concentration, the amount of S proteins removed correlated with the heparin density on the HP-NS surfaces: the higher the heparin density was, the more S proteins were bound and removed. Based on these experimental results, we calculated the nanosponge concentrations needed to remove 50% of S proteins (denoted "IC_{50}") under our experimental conditions (Figure 4B). We found that the IC_{50} values of N_3-NS, HP-NS/L, HP-NS/M, and HP-NS/H were 2.69 ± 0.18, 1.60 ± 0.15, 0.80 ± 0.06, and 0.50 ± 0.02 mg/mL, respectively.

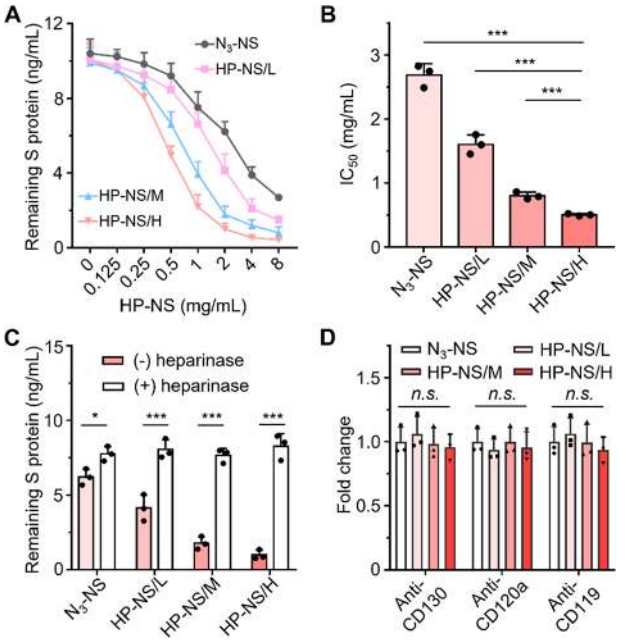

Figure 4. Enhanced binding of SARS-CoV-2 S protein by HP-NS. (A) Dose-dependent binding of various HP-NS formulations with SARS-CoV-2 S proteins. The initial S protein concentration is 10 ng/mL. (B) Corresponding binding IC_{50} values calculated from (A). (C) S protein binding capacity of HP-NS with or without heparinase treatment. The initial S protein concentration was 10 ng/mL. (D) Comparison of cellular nanosponge binding with antibodies against cell membrane surface receptors of three proinflammatory cytokines (IL-6, TNF-α, and IFN-γ). Data presented as mean + s.d. (n = 3); *n.s.*: not significant; ***p < 0.001; statistical analysis by one-way ANOVA.

To verify that the enhanced S protein binding was indeed due to the surface-conjugated heparin, we treated HP-NS formulations (2 mg/mL) with heparinase that selectively cleaved the heparin (Figure 4C). After the enzyme digestion, the HP-NS were washed and collected by centrifugation. In the binding test, the HP-NS without the enzyme treatment showed S protein removal in correlation with their heparin density. In contrast, for all HP-NS formulations with heparinase treatment, S protein concentrations remained high and comparable to the baseline. This experiment confirms the specific role played by the conjugated heparin in binding and removing S proteins. Cellular nanosponges made with THP-1 membranes inhibited SARS-CoV-2 infection by neutralizing multiple factors. For example, nanosponges absorb S proteins through binding receptors such as ACE2 on the membrane.[29] Other receptors such as C type lectin domain family 10 (CLEC 10) and CD147 on the cell membrane may also bind with S proteins for removal.[30] Meanwhile, the membrane also contains various cytokine receptors such as CD120 for TNF-α.[18,31,32] To confirm that heparin conjugation will not impact the binding capability of other cell membrane receptors on the nanosponge surface, we tested nanosponge binding with fluorescently labeled antibodies against proinflammatory cytokine receptors. In the study, phycoerythrin (PE)-labeled anti-CD130 (IL-6 receptor), anti-CD120a (TNF-α receptor), and anti-CD119 (IFN-γ receptor) were incubated with HP-NS or N_3-NS. After the incubation, the nanosponges were removed. Supernatants from all HP-NS formulations showed fluorescence intensities comparable with that of N_3-NS (Figure 4D and Supporting Information Figure S2). The results

https://doi.org/10.1021/jacs.1c07798
J. Am. Chem. Soc. XXXX, XXX, XXX−XXX

confirm that the heparin modification on the cellular nanosponges had a negligible impact on their inherent cytokine binding capabilities.

We next investigated the capability of HP-NS to inhibit SARS-CoV-2 pseudovirus infectivity. In the study, human lung epithelial cells were seeded in 96-well plates the day before the experiment. Serial dilutions of N_3-NS or HP-NS and pseudotyped SARS-CoV-2 were added to the cell monolayers. After 24 h of incubation, the virus-infected cells were determined by the expression of genetically encoded green-fluorescent reporters inside the host cells. As shown in Figure 5A, control cells without adding the viruses or the nanosponges showed no fluorescence. In contrast, cells added with viruses but not nanosponges showed a strong green fluorescence, confirming the viral entry and infection in the epithelial cells. The fluorescence decreased obviously with the addition of N_3-NS or HP-NS, suggesting the inhibition of viral infectivity by the cellular nanosponges. To quantify the inhibition of the infectivity, we varied the concentration of the nanosponges added to the cell culture and measured the fluorescence intensity (Figure 5B). As the amounts of HP-NS increased, the fluorescence intensity from the host cells decreased, indicating a concentration-dependent inhibition effect. The percent of SARS-CoV-2 infectivity was correlated to the amounts of heparin on the HP-NS surfaces at all concentrations: the higher the heparin density, the less the SARS-CoV-2 infectivity. Based on these results, a half-maximal inhibitory concentration (IC_{50}) of HP-NS to inhibit SARS-CoV-2 infectivity under our experimental conditions was calculated (Figure 5C). The IC_{50} values of N_3-NS, HP-NS/L, HP-NS/M, and HP-NS/H were 193 ± 60, 43 ± 24, 17 ± 8, and 6 ± 3 mg/mL, respectively.

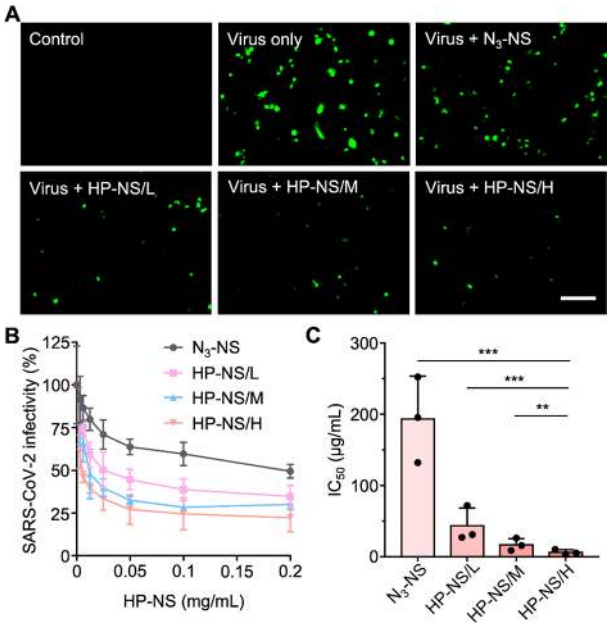

Figure 5. Neutralization of SARS-CoV-2 pseudovirus infectivity by HP-NS. (A) Representative fluorescence images of NL-20 cells without or with HP-NS (25 μg/mL) under the infection of SARS-CoV-2 pseudovirus (5×10^7 viral genes per well) for 24 h. Green represents the fluorescent proteins in the nuclei (scale bars: 100 μm). (B) Dose-dependent inhibition of SARS-CoV-2 infectivity by N_3-NS, HP-NS/L, HP-NS/M, and HP-NS/H. The cells with SARS-CoV-2 infection but without any treatment served as a control of 100% infectivity. (C) Corresponding inhibition IC_{50} values calculated from (B). Data presented as mean + s.d. (n = 3); *n.s.*: not significant; ***p < 0.001; statistical analysis by one-way ANOVA.

Finally, we evaluated the effects of heparin modification on nanosponge neutralization against live SARS-CoV-2 virus. Herein, we selected HP-NS/H (HP-NS lead formulation) and N_3-NS (control group) to perform a plaque reduction neutralization assay.[18] In the study, we first amplified a low-passage sample of SARS-CoV-2 in Vero E6 cells to make a working stock of the virus. Then the Vero E6 cells were seeded at 8×10^5 cells per well in six-well plates the day before the experiment. In the experiment, serial half-log dilutions of the nanosponges starting from 5 mg/mL were mixed with 200 plaque-forming units (PFU) of SARS-CoV-2. The mixture was incubated at 37 °C for 1 h and then added to the cell monolayers followed by another 1 h of incubation. Mock-infected and diluent-only infected wells served as negative and positive controls, respectively. Monolayers were overlaid and incubated for 2 days followed by viral plaque enumeration. Following the incubation, cultures without adding nanosponge samples showed a viral count comparable to that in the negative control, confirming viral entry and infection of the host cells. As shown in Figure 6A, inhibition of the infectivity increased as the concentration of N_3-NS increased, suggesting a dose-dependent neutralization of the live virus. Based on the results, a half-maximal inhibitory concentration (IC_{50}) value of 170 μg/mL for N_3-NS was obtained. In parallel, a similar dose-dependent inhibition of the viral infectivity was observed with HP-NS/H (Figure 6B). In this case, an IC_{50} value of 0.0254 μg/mL was obtained. A significantly lower IC_{50} value of HP-NS/H indicates a much higher potency than N_3-NS, confirming the effect of heparin modification on enhancing SARS-CoV-2 inhibition.

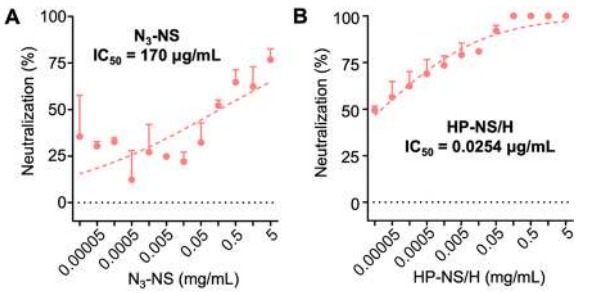

Figure 6. Neutralization of live SARS-CoV-2 infectivity by HP-NS. The neutralization against live SARS-CoV-2 infection by N_3-NS (A) and HP-NS/H (B) was tested on Vero E6 cells. The IC_{50} values for N_3-NS and HP-NS/H were determined to be 170 and 0.0254 μg/mL (membrane protein concentration), respectively. In all data sets, n = 3. Data are presented as mean + standard deviation. Horizontal dashed lines mark the zero levels. IC_{50} values were derived from the variable slope model using Graphpad Prism 8.

CONCLUSIONS

In summary, we showed that increasing the surface heparin density of cellular nanosponges promotes their binding capability with SARS-CoV-2 S proteins and enhances the potency of inhibiting viral infectivity. In our previous work, both wild-type THP-1 cell nanosponges and lung epithelial cell nanosponges inhibited SARS-CoV-2 infectivity with comparable potency. In the current study, we opted for THP-1 cells because their membranes were also able to neutralize various

https://doi.org/10.1021/jacs.1c07798
J. Am. Chem. Soc. XXXX, XXX, XXX−XXX

types of inflammatory cytokines, which would help suppress immune disorders in viral infections.[31,33] Heparin has been shown to enhance S protein binding to ACE2, likely by stabilizing ACE2 during the virus−cell interactions, increasing the proportion of S proteins bound to ACE2, and increasing the occupancy of individual S proteins.[20] Surface modification of cellular nanosponges brought heparin to the proximity of ACE2, allowing the two moieties to cooperate and enhance binding to the viruses. The effect is remarkable, as reflected by over 3 orders of magnitude decrease of the IC_{50} value in live SARS-CoV-2 virus studies.

Besides SARS-CoV-2, other viruses such as dengue-2 virus,[34] Ebola virus,[35] and Zika virus[36] also bind with heparin or heparin sulfate to initiate cell entry. The same glycoengineering approach is also applicable to other glycans such as terminal-linked sialic acid, known as the cellular receptors of viruses such as influenza virus,[37] Middle East respiratory syndrome coronavirus (MERS-CoV),[38] reovirus,[39] and rotavirus.[40] Therefore, increasing the density of these glycans is also anticipated to enhance viral inhibition by the cellular nanosponges. Previous studies using synthetic glycan nanoparticles showed that nanoparticle size and shape affect interligand spacing and thus affect nanoparticle−virus binding affinity.[37] Nanosponges are expected to have similar properties. Therefore, optimizing nanosponge size and shape can be a way to modulate virus binding affinity toward neutralizing different viruses. Specific for lung delivery, some other factors to consider include the margination effect and lung deposition efficiency of the nanosponges. Previous studies also showed the in vivo capability of macrophage nanosponges (made with mouse J774 macrophages) to target multiple organs, including the lungs after intravenous or intraperitoneal injections.[33] Membrane vesicles made from THP-1 macrophages were also tested for inhalation to inhibit SARS-CoV-2 infection.[31] Based on these prior studies, we expect that different nanosponge formulations can be developed for various administration routes, including intravenous injection to neutralize plasma virus and inhalation to target damaged organs such as the lungs. Overall, combining the surface glycan engineering technology with the cellular nanosponges antiviral technology can create new opportunities for developing potent and broad-spectrum antiviral therapeutics.

■ ASSOCIATED CONTENT

Supporting Information

The Supporting Information is available free of charge at https://pubs.acs.org/doi/10.1021/jacs.1c07798.

Experimental description of cell surface metabolic labeling of azido groups, cell membrane derivation, synthesis of DBCO-heparin, fabrication and characterization of N_3-NS and HP-NS, quantification of HP-NS binding with SARS-CoV-2 S proteins, inhibition of SARS-CoV-2 pseudovirus and live virus infection; DBCO conjugation yield (Figure S1) and calculation of binding with cytokine receptor antibodies (Figure S2) (PDF)

■ AUTHOR INFORMATION

Corresponding Authors

Weiwei Gao − *Department of NanoEngineering, Chemical Engineering Program, Moores Cancer Center, University of California San Diego, La Jolla, California 92093, United States*; Email: w5gao@ucsd.edu

Liangfang Zhang − *Department of NanoEngineering, Chemical Engineering Program, Moores Cancer Center, University of California San Diego, La Jolla, California 92093, United States*; orcid.org/0000-0003-0637-0654; Email: zhang@ucsd.edu

Authors

Xiangzhao Ai − *Department of NanoEngineering, Chemical Engineering Program, Moores Cancer Center, University of California San Diego, La Jolla, California 92093, United States*

Dan Wang − *Department of NanoEngineering, Chemical Engineering Program, Moores Cancer Center, University of California San Diego, La Jolla, California 92093, United States*

Anna Honko − *Department of Microbiology and National Emerging Infectious Diseases Laboratories, Boston University School of Medicine, Boston, Massachusetts 02118, United States*; orcid.org/0000-0001-9165-148X

Yaou Duan − *Department of NanoEngineering, Chemical Engineering Program, Moores Cancer Center, University of California San Diego, La Jolla, California 92093, United States*

Igor Gavrish − *Department of Microbiology and National Emerging Infectious Diseases Laboratories, Boston University School of Medicine, Boston, Massachusetts 02118, United States*

Ronnie H. Fang − *Department of NanoEngineering, Chemical Engineering Program, Moores Cancer Center, University of California San Diego, La Jolla, California 92093, United States*

Anthony Griffiths − *Department of Microbiology and National Emerging Infectious Diseases Laboratories, Boston University School of Medicine, Boston, Massachusetts 02118, United States*

Complete contact information is available at: https://pubs.acs.org/10.1021/jacs.1c07798

Author Contributions

[§]X. Ai and D. Wang contributed equally to this work.

Notes

The authors declare no competing financial interest.

■ ACKNOWLEDGMENTS

This work was supported by the Department of the Defense, Defense Threat Reduction Agency, under award number HDTRA1-21-C-0019. The content of the information does not necessarily reflect the position or the policy of the federal government, and no official endorsement should be inferred.

■ REFERENCES

(1) Matheson, N. J.; Lehner, P. J. How does SARS-CoV-2 cause COVID-19? *Science* **2020**, *369*, 510−511.

(2) Zhou, F.; Yu, T.; Du, R. H.; Fan, G. H.; Liu, Y.; Liu, Z. B.; Xiang, J.; Wang, Y. M.; Song, B.; Gu, X. Y.; et al. Clinical course and risk factors for mortality of adult inpatients with COVID-19 in Wuhan, China: a retrospective cohort study. *Lancet* **2020**, *395*, 1054−1062.

(3) Zhu, N.; Zhang, D. Y.; Wang, W. L.; Li, X. W.; Yang, B.; Song, J. D.; Zhao, X.; Huang, B. Y.; Shi, W. F.; Lu, R. J.; et al. A novel coronavirus from patients with pneumonia in China, 2019. *N. Engl. J. Med.* **2020**, *382*, 727−733.

(4) Beigel, J. H.; Tomashek, K. M.; Dodd, L. E.; Mehta, A. K.; Zingman, B. S.; Kalil, A. C.; Hohmann, E.; Chu, H. Y.; Luetkemeyer, A.; Kline, S.; et al. Remdesivir for the treatment of Covid-19-final report. *N. Engl. J. Med.* **2020**, *383*, 1813−1826.
(5) Ledford, H. COVID antibody treatments show promise for preventing severe disease. *Nature* **2021**, *591*, 513−514.
(6) Excler, J. L.; Saville, M.; Berkley, S.; Kim, J. H. Vaccine development for emerging infectious diseases. *Nat. Med.* **2021**, *27*, 591−600.
(7) Fontanet, A.; Autran, B.; Lina, B.; Kieny, M. P.; Karim, S. S. A.; Sridhar, D. SARS-CoV-2 variants and ending the COVID-19 pandemic. *Lancet* **2021**, *397*, 952−954.
(8) Wang, P. F.; Nair, M. S.; Liu, L. H.; Iketani, S.; Luo, Y.; Guo, Y. C.; Wang, M.; Yu, J.; Zhang, B. S.; Kwong, P. D.; et al. Antibody resistance of SARS-CoV-2 variants B.1.351 and B.1.1.7. *Nature* **2021**, *593*, 130−135.
(9) Williams, T. C.; Burgers, W. A. SARS-CoV-2 evolution and vaccines: cause for concern? *Lancet Respir. Med.* **2021**, *9*, 333−335.
(10) Talebian, S.; Wallace, G. G.; Schroeder, A.; Stellacci, F.; Conde, J. Nanotechnology-based disinfectants and sensors for SARS-CoV-2. *Nat. Nanotechnol.* **2020**, *15*, 618−621.
(11) Shin, M. D.; Shukla, S.; Chung, Y. H.; Beiss, V.; Chan, S. K.; Ortega-Rivera, O. A.; Wirth, D. M.; Chen, A.; Sack, M.; Pokorski, J. K.; et al. COVID-19 vaccine development and a potential nanomaterial path forward. *Nat. Nanotechnol.* **2020**, *15*, 646−655.
(12) Tang, Z. M.; Kong, N.; Zhang, X. C.; Liu, Y.; Hu, P.; Mou, S.; Liljestrom, P.; Shi, J. L.; Tan, W. H.; Kim, J. S.; et al. A materials-science perspective on tackling COVID-19. *Nat. Rev. Mater.* **2020**, *5*, 847−860.
(13) Zhou, J.; Krishnan, N.; Jiang, Y.; Fang, R. H.; Zhang, L. Nanotechnology for virus treatment. *Nano Today* **2021**, *36*, 101031.
(14) Rao, L.; Tian, R.; Chen, X. Y. Cell-membrane-mimicking nanodecoys against infectious diseases. *ACS Nano* **2020**, *14*, 2569−2574.
(15) Wei, X. L.; Zhang, G.; Ran, D. N.; Krishnan, N.; Fang, R. H.; Gao, W.; Spector, S. A.; Zhang, L. T-Cell-Mimicking Nanoparticles Can Neutralize HIV Infectivity. *Adv. Mater.* **2018**, *30*, No. e1802233.
(16) Chen, H. W.; Fang, Z. S.; Chen, Y. T.; Chen, Y. I.; Yao, B. Y.; Cheng, J. Y.; Chien, C. Y.; Chang, Y. C.; Hu, C. M. J. Targeting and enrichment of viral pathogen by cell membrane cloaked magnetic nanoparticles for enhanced detection. *ACS Appl. Mater. Interfaces* **2017**, *9*, 39953−39961.
(17) Rao, L.; Wang, W. B.; Meng, Q. F.; Tian, M. F.; Cai, B.; Wang, Y. C.; Li, A. X.; Zan, M. H.; Xiao, F.; Bu, L. L.; et al. A biomimetic nanodecoy traps zika virus to prevent viral infection and fetal microcephaly development. *Nano Lett.* **2019**, *19*, 2215−2222.
(18) Zhang, Q. Z.; Honko, A.; Zhou, J. R.; Gong, H.; Downs, S. N.; Vasquez, J. H.; Fang, R. H.; Gao, W.; Griffiths, A.; Zhang, L. Cellular nanosponges inhibit SARS-CoV-2 infectivity. *Nano Lett.* **2020**, *20*, 5570−5574.
(19) Wang, C.; Wang, S.; Chen, Y.; Zhao, J.; Han, S.; Zhao, G.; Kang, J.; Liu, Y.; Wang, L.; Wang, X.; et al. Membrane nanoparticles derived from ACE2-rich cells block SARS-CoV-2 infection. *ACS Nano* **2021**, *15*, 6340−6351.
(20) Clausen, T. M.; Sandoval, D. R.; Spliid, C. B.; Pihl, J.; Perrett, H. R.; Painter, C. D.; Narayanan, A.; Majowicz, S. A.; Kwong, E. M.; McVicar, R. N.; et al. SARS-CoV-2 infection depends on cellular heparan sulfate and ACE2. *Cell* **2020**, *183*, 1043−1057.
(21) Mycroft-West, C.; Su, D.; Elli, S.; Li, Y.; Guimond, S.; Miller, G.; Turnbull, J.; Yates, E.; Guerrini, M.; Fernig, D.; et al. The 2019 coronavirus (SARS-CoV-2) surface protein (Spike) S1 Receptor Binding Domain undergoes conformational change upon heparin binding.*bioRxiv*, DOI: 10.1101/2020.02.29.971093 (accessed Sept 16, 2021).
(22) Kwon, P. S.; Oh, H.; Kwon, S. J.; Jin, W. H.; Zhang, F. M.; Fraser, K.; Hong, J. J.; Linhardt, R. J.; Dordick, J. S. Sulfated polysaccharides effectively inhibit SARS-CoV-2 in vitro. *Cell Discovery* **2020**, *6*, 50.
(23) Tandon, R.; Sharp, J. S.; Zhang, F. M.; Pomin, V. H.; Ashpole, N. M.; Mitra, D.; Jin, W. H.; Liu, H.; Sharma, P.; Linhardt, R. J.; et al. Effective inhibition of SARS-CoV-2 entry by heparin and enoxaparin derivatives. *J. Virol.* **2021**, *95*, No. e01987.
(24) Takayama, Y.; Kusamori, K.; Nishikawa, M. Click chemistry as a tool for cell engineering and drug delivery. *Molecules* **2019**, *24*, 172.
(25) Fang, R. H.; Hu, C. M. J.; Luk, B. T.; Gao, W.; Copp, J. A.; Tai, Y. Y.; O'Connor, D. E.; Zhang, L. Cancer cell membrane-coated nanoparticles for anticancer vaccination and drug delivery. *Nano Lett.* **2014**, *14*, 2181−2188.
(26) Hu, C. M. J.; Zhang, L.; Aryal, S.; Cheung, C.; Fang, R. H.; Zhang, L. Erythrocyte membrane-camouflaged polymeric nanoparticles as a biomimetic delivery platform. *Proc. Natl. Acad. Sci. U. S. A.* **2011**, *108*, 10980−10985.
(27) Xu, J. W.; Feng, E.; Song, J. Bioorthogonally cross-linked hydrogel network with precisely controlled disintegration time over a broad range. *J. Am. Chem. Soc.* **2014**, *136*, 4105−4108.
(28) Barker, K.; Rastogi, S. K.; Dominguez, J.; Cantu, T.; Brittain, W.; Irvin, J.; Betancourt, T. Biodegradable DNA-enabled poly-(ethylene glycol) hydrogels prepared by copper-free click chemistry. *J. Biomater. Sci., Polym. Ed.* **2016**, *27*, 22−39.
(29) Yan, R. H.; Zhang, Y. Y.; Li, Y. N.; Xia, L.; Guo, Y. Y.; Zhou, Q. Structural basis for the recognition of SARS-CoV-2 by full-length human ACE2. *Science* **2020**, *367*, 1444−1448.
(30) Qi, F. R.; Qian, S.; Zhang, S. Y.; Zhang, Z. Single cell RNA sequencing of 13 human tissues identify cell types and receptors of human coronaviruses. *Biochem. Biophys. Res. Commun.* **2020**, *526*, 135−140.
(31) Rao, L.; Xia, S.; Xu, W.; Tian, R.; Yu, G. C.; Gu, C. J.; Pan, P.; Meng, Q. F.; Cai, X.; Qu, D.; et al. Decoy nanoparticles protect against COVID-19 by concurrently adsorbing viruses and inflammatory cytokines. *Proc. Natl. Acad. Sci. U. S. A.* **2020**, *117*, 27141−27147.
(32) Hehlgans, T.; Pfeffer, K. The intriguing biology of the tumour necrosis factor/tumour necrosis factor receptor superfamily: players, rules and the games. *Immunology* **2005**, *115*, 1−20.
(33) Thamphiwatana, S.; Angsantikul, P.; Escajadillo, T.; Zhang, Q. Z.; Olson, J.; Luk, B. T.; Zhang, S.; Fang, R. H.; Gao, W.; Nizet, V.; et al. Macrophage-like nanoparticles concurrently absorbing endotoxins and proinflammatory cytokines for sepsis management. *Proc. Natl. Acad. Sci. U. S. A.* **2017**, *114*, 11488−11493.
(34) Lin, Y. L.; Lei, H. Y.; Lin, Y. S.; Yeh, T. M.; Chen, S. H.; Liu, H. S. Heparin inhibits dengue-2 virus infection of five human liver cell lines. *Antiviral Res.* **2002**, *56*, 93−96.
(35) Tamhankar, M.; Gerhardt, D. M.; Bennett, R. S.; Murphy, N.; Jahrling, P. B.; Patterson, J. L. Heparan sulfate is an important mediator of Ebola virus infection in polarized epithelial cells. *Virol. J.* **2018**, *15*, 135.
(36) Ghezzi, S.; Cooper, L.; Rubio, A.; Pagani, I.; Capobianchi, M. R.; Ippolito, G.; Pelletier, J.; Meneghetti, M. C. Z.; Lima, M. A.; Skidmore, M. A.; et al. Heparin prevents Zika virus induced-cytopathic effects in human neural progenitor cells. *Antiviral Res.* **2017**, *140*, 13−17.
(37) Kwon, S. J.; Na, D. H.; Kwak, J. H.; Douaisi, M.; Zhang, F.; Park, E. J.; Park, J. H.; Youn, H.; Song, C. S.; Kane, R. S.; et al. Nanostructured glycan architecture is important in the inhibition of influenza A virus infection. *Nat. Nanotechnol.* **2017**, *12*, 48−54.
(38) Li, W. T.; Hulswit, R. J. G.; Widjaja, I.; Raj, V. S.; McBride, R.; Peng, W. J.; Widagdo, W.; Tortorici, M. A.; van Dieren, B.; Lang, Y.; et al. Identification of sialic acid-binding function for the Middle East respiratory syndrome coronavirus spike glycoprotein. *Proc. Natl. Acad. Sci. U. S. A.* **2017**, *114*, E8508−E8517.
(39) Connolly, J. L.; Barton, E. S.; Dermody, T. S. Reovirus binding to cell surface sialic acid potentiates virus-induced apoptosis. *J. Virol.* **2001**, *75*, 4029−4039.
(40) Isa, P.; Arias, C. F.; Lopez, S. Role of sialic acids in rotavirus infection. *Glycoconjugate J.* **2006**, *23*, 27−37.

https://doi.org/10.1021/jacs.1c07798
J. Am. Chem. Soc. XXXX, XXX, XXX−XXX